Syntheses, Structures, Second-Harmonic Generating, and Ferroelectric Properties of Tungsten Bronzes: $A_6M_2M'_8O_{30}$ ($A = Sr^{2+}$, Ba^{2+}, or Pb^{2+}; $M = Ti^{4+}$, Zr^{4+}, or Hf^{4+}; $M' = Nb^{5+}$ or Ta^{5+})

Eun Ok Chi,[†] Alberto Gandini,[‡] Kang Min Ok,[†] Lei Zhang,[†] and P. Shiv Halasyamani*,[†]

Department of Chemistry and Center for Materials Chemistry, University of Houston, 136 Fleming Building, Houston, Texas 77204-5003, and Department of Physics, University of Houston, Science and Research 1 Building, Houston, TX, 77005-5005

Received May 14, 2004

Nine tungsten bronze oxides, $A_6M_2M'_8O_{30}$ ($A = Sr^{2+}$, Ba^{2+}, or Pb^{2+}; $M = Ti^{4+}$, Zr^{4+}, or Hf^{4+}; $M' = Nb^{5+}$ or Ta^{5+}), have been synthesized and characterized. Although structurally very similar, the nine materials are not isostructural. The materials crystallize in noncentrosymmetric space groups, *P4bm* (no. 100) for $Ba_6Ti_2Nb_8O_{30}$, $Ba_6Ti_2Ta_8O_{30}$, $Ba_6Zr_2Nb_8O_{30}$, $Ba_6Zr_2Ta_8O_{30}$, $Ba_6Hf_2Nb_8O_{30}$, and $Ba_6Hf_2Ta_8O_{30}$; *Pba*2 (no. 52) for $Sr_6Ti_2Nb_8O_{30}$ and $Sr_6Ti_2Ta_8O_{30}$; and *Cm*2*m* (no. 38) for $Pb_6Ti_2Nb_8O_{30}$. All of the compounds exhibit second-order nonlinear optical behavior, i.e., second-harmonic generation (SHG), by frequency doubling 1064 nm radiation to 532 nm. The SHG efficiencies range from 10 to 600 × SiO_2. The reported materials are also ferroelectric, as demonstrated by hysteresis loops (polarization vs electric field). Spontaneous polarization values (P_s) range from 0.79 to 12.1 $\mu C/cm^2$. The magnitude of the SHG efficiency and ferroelectric polarization are strongly dependent on the A, M, and M′ cations.

Introduction

Tungsten bronze oxides have been studied extensively owing to their fascinating structural chemistry and technologically relevant physical properties.[1−4] The tungsten bronze structure consists of a corner-sharing framework of MO_6 octahedra (M = Ti, Nb, Ta, or W) that contain interstitial sites where a variety of metal cations may reside. As reported earlier and extensively discussed, the bronze family can be divided into three groups.[5] The nonstoichiometric, highly colored bronzes; compounds of the type $(AO)_x(B_2O_5)$ (A = Na, K, Sr, Ba, or Pb; B = Nb, Ta, or W); and materials with a general formula $(A1)_2(A2)_4C_4(B1)_2(B2)_8O_{30}$. We will be focusing on the latter type of materials, and since a detailed description has been given,[5] we will only give a brief account here. The archetypal structure for the $(A1)_2(A2)_4C_4(B1)_2(B2)_8O_{30}$ stoichiometry is shown in Figure 1. As seen in Figure 1, the A, B, and C cations occupy specific sites in the structure and are restricted to certain cations. Cations found in the A site must be able to accommodate large oxide coordination numbers—greater than nine. Thus, this site is restricted to larger alkali, alkaline earth, and Pb cations. Cations on the B site are in an octahedral coordination environment. Thus, transition metal cations such as Ti^{4+}, Nb^{5+}, Ta^{5+},

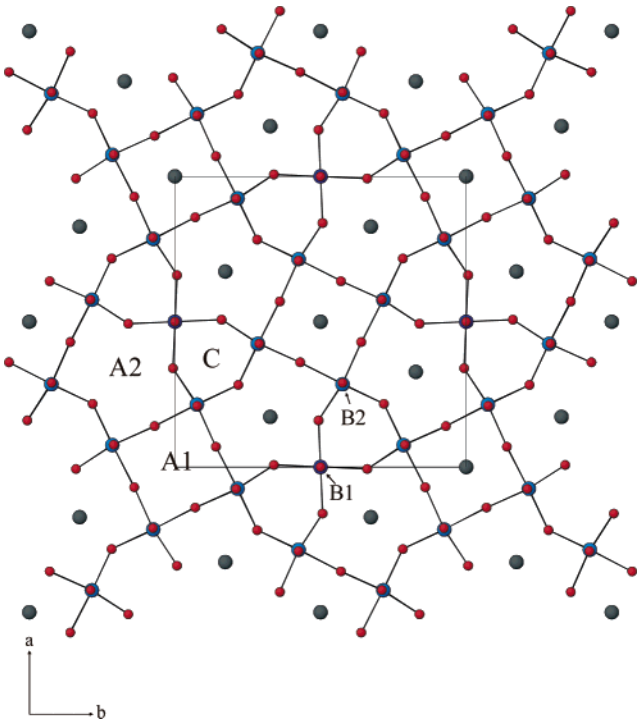

Figure 1. Archetypal tungsten bronze framework indicating the corner-shared oxide octahedra (B1 and B2 sites), as well as the larger (A1 and A2) and smaller (C) sites.

[†] Department of Chemistry and Center for Materials Chemistry.
[‡] Department of Physics.

(1) Lenzo, P. V.; Spenser, E. G.; Ballman, A. A. *Appl. Phys. Lett.* **1967**, *11*, 23−24.
(2) Itoh, Y.; Iwasaki, H. *J. Phys. Chem. Solids* **1972**, *34*, 1639−1645.
(3) Liu, S. T.; Maciolek, R. B. *J. Electron. Mater.* **1975**, *4*, 91−100.
(4) Neurgaonkar, R. R.; Nelson, J. G.; Oliver, J. R. *Mater. Res. Bull.* **1992**, *27*, 677−684.
(5) Jamieson, P. B.; Abrahams, S. C.; Bernstein, J. L. *J. Chem. Phys.* **1968**, *48*, 5048−5057.

10.1021/cm049234y CCC: $27.50
Published on Web 08/26/2004

and W^{6+} are commonly observed. Finally, cations on the C site are necessarily small, given the restricted coordination environment, and to date only Li^+ and small rare earth ions such as Er^{3+} and Lu^{3+} has been observed occupying this site.[6,7]

In addition to the rich structural chemistry, tungsten bronzes have a number of important and interesting physical properties, including second-order nonlinear optical behavior (second-harmonic generation), ferroelectricity, pyroelectricity, and piezoelectricity.[1,3,8] These properties are attributable to the noncentrosymmetric, often polar, nature of the materials and, more specifically, the intraoctahedral distortion of the B cation (Ti^{4+}, Nb^{5+}, W^{6+}, etc.). This out-of-center distortion can be attributed to second-order Jahn−Teller (SOJT) effects.[9−15] SOJT effects occur when the empty d-orbitals of the metal mix with the filled p-orbitals of the ligands. In extended structures, this mixing results in a host of nearly degenerate electronic configurations. These degenerate configurations can be removed through the spontaneous distortion of the d^0 transition metal. This out-of-center distortion has a profound influence with respect to the associated physical properties, specifically second-harmonic generation (SHG) and ferroelectric behavior. A number of bronzes have been reported to have strong SHG efficiencies, $>400 \times SiO_2$.[1,16] These strong efficiencies are attributable to not only the large β(M−O) (metal−oxygen hyperpolarizability), where M is a d^0 transition metal, but also the "constructive alignment" of these hyperpolarizabilities. The second physical property often associated with tungsten bronzes is ferroelectricity. Formally, all ferroelectric materials are pyroelectric,[17] i.e., a material with a permanent dipole moment, with reversible polarization.[18] The symmetry requirements for ferroelectricity are much more restrictive compared to SHG. A ferroelectric material *must* crystallize in one of 10 polar crystal classes (1, 2, 3, 4, 6, *m*, *mm*2, 3*m*, 4*mm*, or 6*mm*).[19] Being found in a polar crystal class, however, is a necessary but not sufficient condition for ferroelectric behavior. The observed dipole moment in these materials must be switchable in the presence of an external electric field. This ferroelectric hysteresis loop (polarization vs electric field) has only been measured on a few of these bronzes, but it is the single most important measurement for a ferroelectric material.[20] With this measurement the spontaneous (P_s) and remnant (P_r) polarization can be measured. A second phenomenon often observed in ferroelectrics is a maximum in the dielectric constant at the Curie temperature (T_c). At the T_c, the material undergoes a phase-change to a nonpolar, often called paraelectric, state. [The term paraelectric has often been used to describe the nonpolar, centrosymmetric state of a ferroelectric (above the T_c). This term is based on the analogy between ferromagnets and ferroelectrics, in the sense that hysteresis loops can be measured for each phenomenon. However, to continue the analogy is inaccurate. Whereas a para*magnet* has a magnetic moment, a para*electric* has *no* electric (dipole) moment. We prefer the term nonpolar, rather than paraelectric, to describe the centrosymmetric state. It is true, however, that noncentrosymmetric nonpolar materials can exist, i.e., chiral compounds. By symmetry, these materials cannot be ferroelectric.] Often, however, the T_c occurs above the melting point or decomposition temperature of the material.

In this paper, we report on the synthesis and characterization of nine tungsten bronze oxides, $A_6M_2M'_8O_{30}$ (A = Sr^{2+}, Ba^{2+}, or Pb^{2+}; M = Ti^{4+}, Zr^{4+}, or Hf^{4+}; M′ = Nb^{5+} or Ta^{5+}). With respect to the formula given earlier, Sr^{2+}, Ba^{2+}, and Pb^{2+} occupy the A1 and A2 sites, whereas the M and M′ cations are randomly disordered over the B1 and B2 sites. The C sites are unoccupied. These materials have been structurally examined by room-temperature X-ray or neutron powder diffraction (Pb^{2+} phase) and characterized by powder SHG, dielectric, and polarization measurements. All of the materials are SHG active and are ferroelectric as demonstrated by hysteresis (polarization vs electric field) loops. We will demonstrate the importance of the A, M, and M′ cations for the SHG and ferroelectric properties.

Experimental Section

Polycrystalline samples of $Sr_6Ti_2Nb_8O_{30}$, $Sr_6Ti_2Ta_8O_{30}$, $Ba_6Ti_2Nb_8O_{30}$, $Ba_6Ti_2Ta_8O_{30}$, $Ba_6Zr_2Nb_8O_{30}$, $Ba_6Zr_2Ta_8O_{30}$, $Ba_6Hf_2Nb_8O_{30}$, $Ba_6Hf_2Ta_8O_{30}$, and $Pb_6Ti_2Nb_8O_{30}$ were prepared by conventional solid-state reactions. Stoichiometric amounts of corresponding metal carbonates or PbO, TiO_2, ZrO_2, HfO_2, Nb_2O_5, and Ta_2O_5, were ground, calcined at 1000 °C for 30 h, and pressed into pellets. For all of the compounds except $Pb_6Ti_2Nb_8O_{30}$, the pellets were heated in air to 1250−1450 °C for 60 h with intermittent regrindings. For $Pb_6Ti_2Nb_8O_{30}$, the pellet was heated to 1250 °C and cooled rapidly by turning off the furnace. $Pb_6Ti_2Nb_8O_{30}$ is reported to have a pyrochlore rather than a tungsten bronze structure.[4] With our experiments, the pyrochlore structure was observed at lower temperatures (<1200 °C). At higher temperatures, however, $Pb_6Ti_2Nb_8O_{30}$ forms a tungsten bronze with a structure similar to $PbNb_2O_6$.[21]

X-ray powder diffraction data were collected using a Scintag XDS2000 diffractometer equipped with Cu Kα radiation. The 2θ range was 5°−120° with a step size of 0.02° and a fixed time of 10 s. Rietveld refinement was performed using the Fullprof program.[22] Six background parameters of Chebyshev polynomial, pseudo-Voigt peak shape function, and asymmetry parameters were included in the refinement process. Time-

(6) Bonner, W. A.; Grodkiewicz, W. H.; Uitert, L. G. *J. Cryst. Growth* **1967**, *1*, 318.
(7) Neurgaonkar, R. R.; Nelson, J. G.; Oliver, J. R.; Cross, L. E. *Mater. Res. Bull.* **1990**, *25*, 959.
(8) Glass, A. M. *J. Appl. Phys.* **1969**, *40*, 4699−4713.
(9) Opik, U.; Pryce, M. H. L. *Proc. R. Soc. (London)*, **1957**, *A238*, 425−447.
(10) Bader, R. F. W. *Mol. Phys.* **1960**, *3*, 137−151.
(11) Bader, R. F. W. *Can. J. Chem.* **1962**, *40*, 1164−1175.
(12) Pearson, R. G. *J. Am. Chem. Soc.* **1969**, *91*, 4947−4955.
(13) Pearson, R. G. *J. Mol. Structure (THEOCHEM)* **1983**, *103*, 25−34.
(14) Wheeler, R. A.; Whangbo, M.-H.; Hughbanks, T.; Hoffmann, R.; Burdett, J. K.; Albright, T. A. *J. Am. Chem. Soc.* **1986**, *108*, 2222−2236.
(15) Kunz, M.; Brown, I. D. *J. Solid State Chem.* **1995**, *115*, 395−406.
(16) Xu, Y. *Ferroelectric Materials and their Applications*; Elsevier Science: Amsterdam, 1991.
(17) Lang, S. B. *Sourcebook of Pyroelectricity*; Gordon & Breach Science: London, 1974.
(18) Jona, F.; Shirane, G. *Ferroelectric Crystals*; Pergamon Press: Oxford, 1962.
(19) Halasyamani, P. S.; Poeppelmeier, K. R. *Chem. Mater.* **1998**, *10*, 2753.
(20) Haertling, G. H. *Electro-optic Ceramics and Devices*; Levinson, L. M., Ed.; Marcel Dekker: New York, 1988; pp 371−492.
(21) Labbe, P. P.; Frey, M.; Allais, G. *Acta Crystallogr.* **1973**, *B29*, 2204.
(22) Rodriguez, J. C. *FULLPROF program: Rietveld Pattern Matching Analysis of Powder Patterns, ILL*, Grenoble; 1998.

Table 1. Summary of Crystallographic Data and Refinement Results for $A_6M_2M'_8O_{30}$ ($A = Sr^{2+}$, Ba^{2+}, or Pb^{2+}; $M = Ti^{4+}$, Zr^{4+}, or Hf^{4+}; $M' = Nb^{5+}$ or Ta^{5+})

	$Sr_6Ti_2Nb_8O_{30}$	$Sr_6Ti_2Ta_8O_{30}$	$Ba_6Ti_2Nb_8O_{30}$	$Ba_6Ti_2Ta_8O_{30}$	$Ba_6Zr_2Nb_8O_{30}$	$Ba_6Zr_2Ta_8O_{30}$	$Ba_6Hf_2Nb_8O_{30}$	$Ba_6Hf_2Ta_8O_{30}$	$Pb_6Ti_2Nb_8O_{30}$[a]
a (Å)	12.3647(3)	12.3660(3)	12.5301(2)	12.5653(2)	12.6811(1)	12.6967(1)	12.6710(3)	12.6629(6)	17.6980(6)
b (Å)	12.4039(3)	12.4020(3)	12.5301(2)	12.5653(2)	12.6811(1)	12.6967(1)	12.6710(3)	12.6629(6)	18.0093(6)
c (Å)	3.8782(1)	3.86712(8)	4.01000(8)	3.95680(6)	4.0173(1)	3.99620(6)	4.0123(1)	3.9830(2)	3.8852(1)
sp grp	*Pba*2	*Pba*2	*P*4*bm*	*P*4*bm*	*P*4*bm*	*P*4*bm*	*P*4*bm*	*P*4*bm*	*Cm*2*m*
R_p[b]	12.6	8.18	12.4	8.64	12.2	8.51	10.4	9.35	5.47
R_{wp}[c]	16.8	10.5	17.7	11.5	16.8	11.4	14.4	12.3	7.35

[a] Room-temperature neutron diffraction data. [b] $R_p = 100\sum|I_o - I_c|/\sum|I_o|$. [c] $R_{wp} = 100(\sum w|I_o - I_c|^2/\sum w|I_o|^2)^{1/2}$.

of-flight (TOF) neutron diffraction data for $Pb_6Ti_2Nb_8O_{30}$ were collected on the general purpose powder diffractometer (GPPD) at Argonne's Intense Pulsed Neutron Source (IPNS). Rietveld profile analysis was performed with the program GSAS.[23] Powder SHG measurements were performed on a modified Kurtz-NLO system[24] using a pulsed Nd:YAG laser with a wavelength of 1064 nm. A detailed description of the equipment and the methodology used has been published.[25,26] Since the SHG efficiency has been shown to depend strongly on particle size, polycrystalline samples were ground and sieved into distinct particle size ranges. To make relevant comparisons with known SHG materials, crystalline SiO_2 and $LiNbO_3$ were also ground and sieved into the same particle size ranges. No index matching fluid was used in any of the experiments. For the dielectric measurements, a Hewlett-Packard low-frequency impedance analyzer (HP4192A) in the 5−13 MHz frequency range was used. Variable temperature (−180 to 450 °C) dielectric measurements were performed by using a Linkam THMSE600 hot stage. All of the samples were sintered, $^1/_2$ in. diameter, and approximately 1 mm thick pellets with conducting silver paste applied to both sides for electrodes. Ferroelectric hysteresis loops were measured on a Radiant Technologies RT66A ferroelectric test system with a TREK high voltage amplifier. A maximum voltage of 4000 V was applied to the samples.

Structural Characterization. The structures for all of the phases except $Pb_6Ti_2Nb_8O_{30}$ were solved from laboratory powder X-ray data. For $Pb_6Ti_2Nb_8O_{30}$, we were unable to satisfactorily determine the structure from laboratory powder X-ray data. Thus, TOF neutron diffraction data were collected at room temperature. Table 1 gives a summary of the crystallographic data for the materials reported in this paper. For all of the refinements except $Pb_6Ti_2Nb_8O_{30}$, the M (Ti^{4+}, Zr^{4+}, and Hf^{4+}) and M′ (Nb^{5+} and Ta^{5+}) cations were disordered over the B1 and B2 sites, with occupancies constrained to produce a $M_2M'_8$ stoichiometry. With $Sr_6Ti_2Nb_8O_{30}$, a structure in the orthorhombic space group *Cmm*2 with a unit cell of $a \sim \sqrt{2}a_t$, $b \sim \sqrt{2}a_t$, and $c = 2c_t$, where a_t and c_t are the tetragonal unit cell from $Ba_6Ti_2Nb_8O_{30}$, has been suggested.[4] Space groups *Cmm*2 and *Pba*2 are two orthorhombic subgroups of *P*4*bm*. In the published work, only an indexed unit cell was given. We did not observe any superstructure peak corresponding to the suggested cell in space group *Cmm*2, and refinements in space group *Cmm*2 with the previously reported cell resulted in unsatisfactory fits. In addition, we were able to index and refine $Sr_6Ti_2Nb_8O_{30}$ and $Sr_6Ti_2Ta_8O_{30}$ on different orthorhombic cells in space group *Pba*2 (see Table 1). The single-crystal structure of $Ba_6Ti_2Nb_8O_{30}$ has been reported,[5] and our powder refinement confirmed the published structure ($a = b =$ 12.5301(2) Å, $c =$ 4.01000(8) Å, and space group *P*4*bm* (see Table 1). The remaining $Ba_6M_2M'_8O_{30}$ phases are isostructural to $Ba_6Ti_2Nb_8O_{30}$, and refinements for these materials proceeded satisfactorily. For $Pb_6Ti_2Nb_8O_{30}$, a cubic pyrochlore structure is synthesized at temperatures below 1200 °C. Above this temperature, however, a tungsten bronze structure is formed. All of the peaks for $Pb_6Ti_2Nb_8O_{30}$ could be indexed on an orthorhombic tungsten bronze structure with a unit cell of $a \sim \sqrt{2}a_t$, $b \sim \sqrt{2}a_t$, and $c = 2c_t$ and pyrochlore impurity (*Fd*-3*m*, centrosymmetric space group). $Pb_6Ti_2Nb_8O_{30}$ has six unique M/M′ sites. During the refinement a restraint was included such that the occupancies of the cations summed to 1.0, i.e., M(occ) + M′(occ) = 1.0. The overall resulting occupancy, M:M′ = 1.90(9):8.10(9), is in good agreement with the $M_2M'_8$ stoichiometry. The experimental, calculated, and difference plots for all nine materials have been deposited as Supporting Information. Also, the atomic coordinates and thermal parameters for the reported materials have been deposited.

Results

Although the nine materials reported in this paper exhibit tungsten bronze-type structures, all of the compounds are not isostructural. All of the phases consist of corner-shared $MO_6/M'O_6$ octahedra, with the M and M′ cations randomly disordered over the B1 and B2 sites (see Figure 1). The Sr^{2+} and Ba^{2+} cations reside in the center of the A1 and A2 sites (see Figure 1), whereas the Pb^{2+} cations are shifted to one side of these sites, attributable to its lone pair (see Figure 2). For all the reported materials the C sites are empty. As we will demonstrate, the different A, M, and M′ cations profoundly influence the observed physical properties. The cation on the A1 and A2 sites are 12- and 15-coordinate, respectively. For Sr^{2+} the ionic radii[27] for these coordination numbers are 1.44 and 1.56 Å, respectively, whereas for Ba^{2+} (Pb^{2+}) the analogous values are 1.61 Å (1.49 Å) and 1.73 Å (1.71 Å), respectively. We suggest that the smaller Sr^{2+} cation compared with Ba^{2+} and Pb^{2+} allows for more structural flexibility in $Sr_6Ti_2Nb_8O_{30}$ and $Sr_6Ti_2Ta_8O_{30}$, and results in a reduction of symmetry to orthorhombic. The larger Ba^{2+} cation imparts rigidity to the metal oxide framework, resulting in a tetragonal structure. Thus, $Ba_6M_2M'_8O_{30}$ ($M = Ti^{4+}$, Zr^{4+}, or Hf^{4+}; $M' = Nb^{5+}$ or Ta^{5+}) are isostructural and crystallize in the tetragonal space group *P*4*bm*. The addition of a lone-pair active cation, Pb^{2+}, on the A1 and A2 sites also changes the symmetry of $Pb_6Ti_2Nb_8O_{30}$ to orthorhombic, space group *Cm*2*m*. Additionally, unlike the Sr^{2+} and Ba^{2+} phases, the Pb^{2+} cation does not reside in the center of the A sites, but rather the Pb^{2+} cation sits to one side of the five- and four-member rings, allowing space for the lone pair (see Figure 2).

The M/M′−O bond lengths for all of the reported compounds have been deposited as Supporting Information. The M and M′ cations undergo an out-of-center distortion, resulting in a range of M/M′−O bond lengths. The direction and magnitude of these displacements, however, are not identical. For $Sr_6Ti_2Nb_8O_{30}$ and $Sr_6Ti_2Ta_8O_{30}$ there are three unique M/M′ sites. With

(23) Larson, A. C.; Von Dreele, R. B. *Report No. LA-UR-86-748*; Los Alamos National Laboratory: Los Alamos, NM, 1987.
(24) Kurtz, S. K.; Perry, T. T. *J. Appl. Phys.* **1968**, *39*, 3798.
(25) Porter, Y.; Ok, K. M.; Bhuvanesh, N. S. P.; Halasyamani, P. S. *Chem. Mater.* **2001**, *13*, 1910.
(26) Ok, K. M.; Bhuvanesh, N. S. P.; Halasyamani, P. S. *J. Solid State Chem.* **2001**, *161*, 57.
(27) Shannon, R. D. *Acta Crystallogr.* **1976**, *A32*, 751.

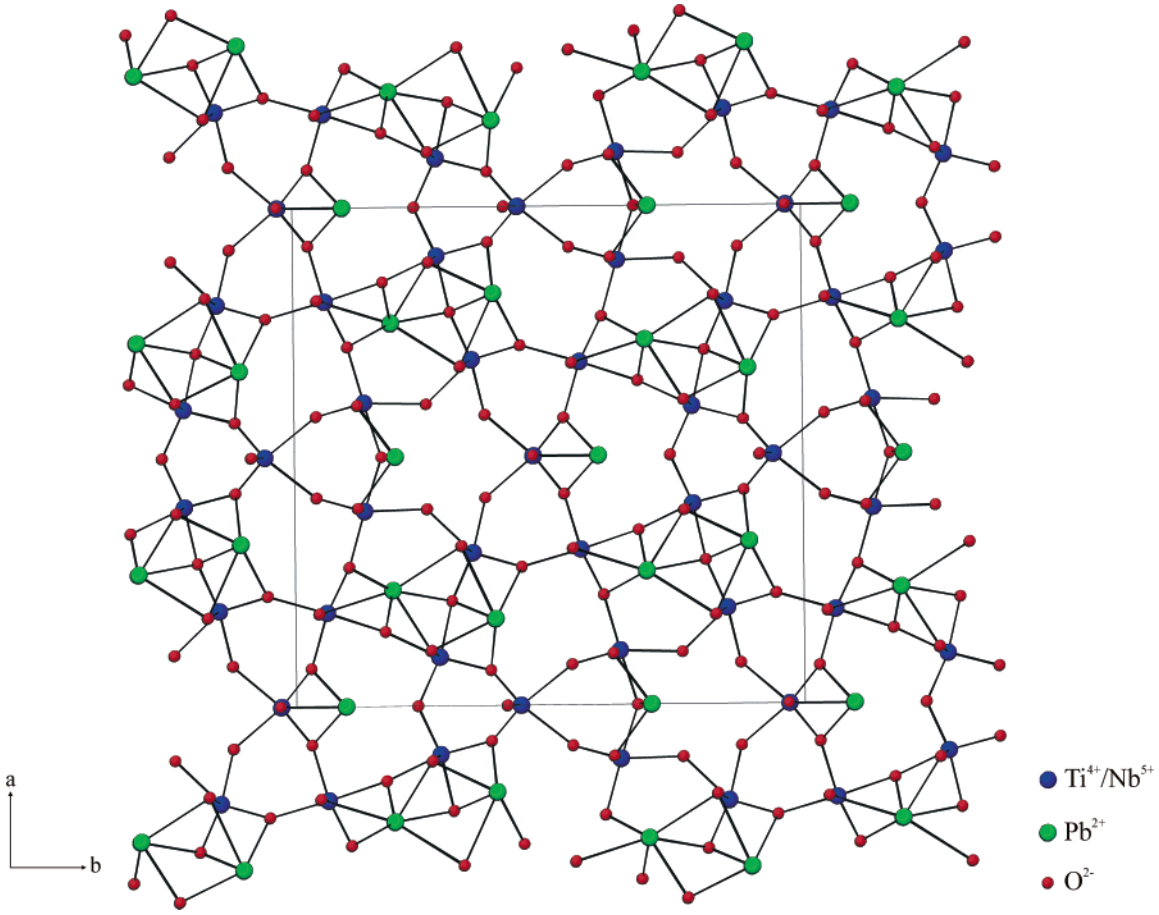

Figure 2. Ball-and-stick representation of $Pb_6Ti_2Nb_8O_{30}$ in the *ab*-plane. Note that the Pb^{2+} cations are off-center in the A1 and A2 sites.

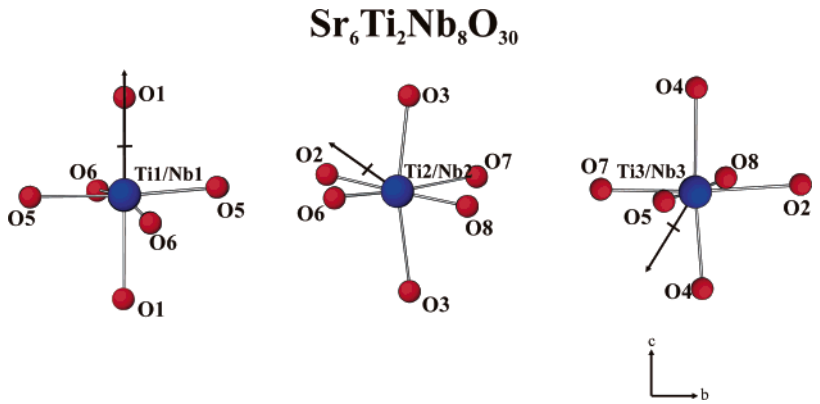

Figure 3. Ball-and-stick representations of the out-of-center distortions of the three unique Ti^{4+}/Nb^{5+} cations in $Sr_6Ti_2Nb_8O_{30}$. The arrow represents the approximate direction of the local moment in each octahedron.

respect to the direction of the out-of-center distortion, only one of the three unique cations, Ti1/Nb1 and Ti1/Ta1 for $Sr_6Ti_2Nb_8O_{30}$ and $Sr_6Ti_2Ta_8O_{30}$, displaces toward a corner (C_4) along the polar [001] direction. The other two cations displace toward a face (C_3), along the [−1−11] and [−11−1] directions (see Figure 3). Thus the net polarization for these materials is along the approximate [−101] direction. With respect to the magnitude of the distortions, the Ti/Nb cations are found to distort to a greater extent compared with the Ti/Ta cations. Additionally, the magnitudes of the corner and face distortions, within each material, are roughly equal.

With $Ba_6Ti_2Nb_8O_{30}$, $Ba_6Ti_2Ta_8O_{30}$, $Ba_6Zr_2Nb_8O_{30}$, $Ba_6Zr_2Ta_8O_{30}$, $Ba_6Hf_2Nb_8O_{30}$, and $Ba_6Hf_2Ta_8O_{30}$, a different situation is observed. For these materials only two unique M/M′ occur in each structure. For these phases, both of the M/M′ cations displace toward a corner (one more so than the other), along the [001] direction (see Figure 4). The magnitude of the out-of-center distortion is larger for one cation compared with the other; thus, the net direction of the polarization is effectively along the [001] direction.

With $Pb_6Ti_2Nb_8O_{30}$, we have two different types of polarizable cations, the d^0 transition metals, Ti^{4+}/Nb^{5+}, and the lone-pair cation, Pb^{2+} (see Figure 2). In addition,

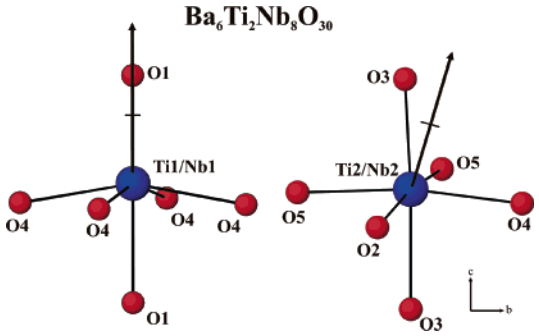

Figure 4. Ball-and-stick representations of the out-of-center distortions of the two unique Ti^{4+}/Nb^{5+} cations in $Ba_6Ti_2Nb_8O_{30}$. The arrow represents the approximate direction of the local moment in each octahedron.

there are six unique Ti/Nb sites. The Ti^{4+}/Nb^{5+} cations distort toward an edge (C_2) either along the [010] or [100] direction, with roughly equal magnitude. With the four unique Pb^{2+} cations, we observe a lone pair that places each PbO_x ($x = 5-9$) polyhedra in an asymmetric coordination environment. The polarizations are observed to occur along the [010] and [0−10] directions. The net polarization attributable to the Pb^{2+} is, however, not zero. In fact, if we add all of the moments attributable to the PbO_x polyhedra, we observe a moment along the [010] direction. If we combine the Pb^{2+} moments with the polarizations associated with the Ti^{4+}/Nb^{5+} cations, we observe a net moment approximately along the [010] direction (see Figure 5). As we will demonstrate with all of the reported materials, the direction and magnitude of the distortions in the M, M′, and A cations profoundly influence the second-harmonic generating and ferroelectric properties.

Second-Harmonic Generation. All of the reported materials crystallize in noncentrosymmetric space groups, *Pba*2 (Sr^{2+} phases), *P*4*bm* (Ba^{2+} phases), and *Cm*2*m* (Pb^{2+} phases). These space groups not only exhibit the proper symmetry for SHG behavior but are also polar, indicating possible ferroelectric behavior (see below). Powder SHG measurements on the reported materials revealed SHG efficiencies ranging from 10 to 600 × SiO_2. We also determined the type 1 phase-matching capability (PM = phase-matchable and NPM = non-phase-matchable) of the materials by measuring the SHG as a function of particle size (20−120 μm). In doing so we were able to calculate $\langle d_{eff} \rangle$, the bulk NLO efficiency, for each material (see table below). The particle size vs SHG efficiency curves for all nine materials have been deposited in the Supporting Information.

compound	SHG (vs SiO_2)	$\langle d_{eff} \rangle$ (pm/V)
$Sr_6Ti_2Nb_8O_{30}$ (NPM)	20	2.5
$Sr_6Ti_2Ta_8O_{30}$ (NPM)	10	1.7
$Ba_6Ti_2Nb_8O_{30}$ (NPM)	500	12.3
$Ba_6Ti_2Ta_8O_{30}$ (NPM)	10	1.7
$Ba_6Zr_2Nb_8O_{30}$ (NPM)	300	9.6
$Ba_6Zr_2Ta_8O_{30}$ (NPM)	10	1.7
$Ba_6Hf_2Nb_8O_{30}$ (NPM)	50	3.9
$Ba_6Hf_2Ta_8O_{30}$ (NPM)	10	1.7
$Pb_6Ti_2Nb_8O_{30}$ (PM)	600	28.2

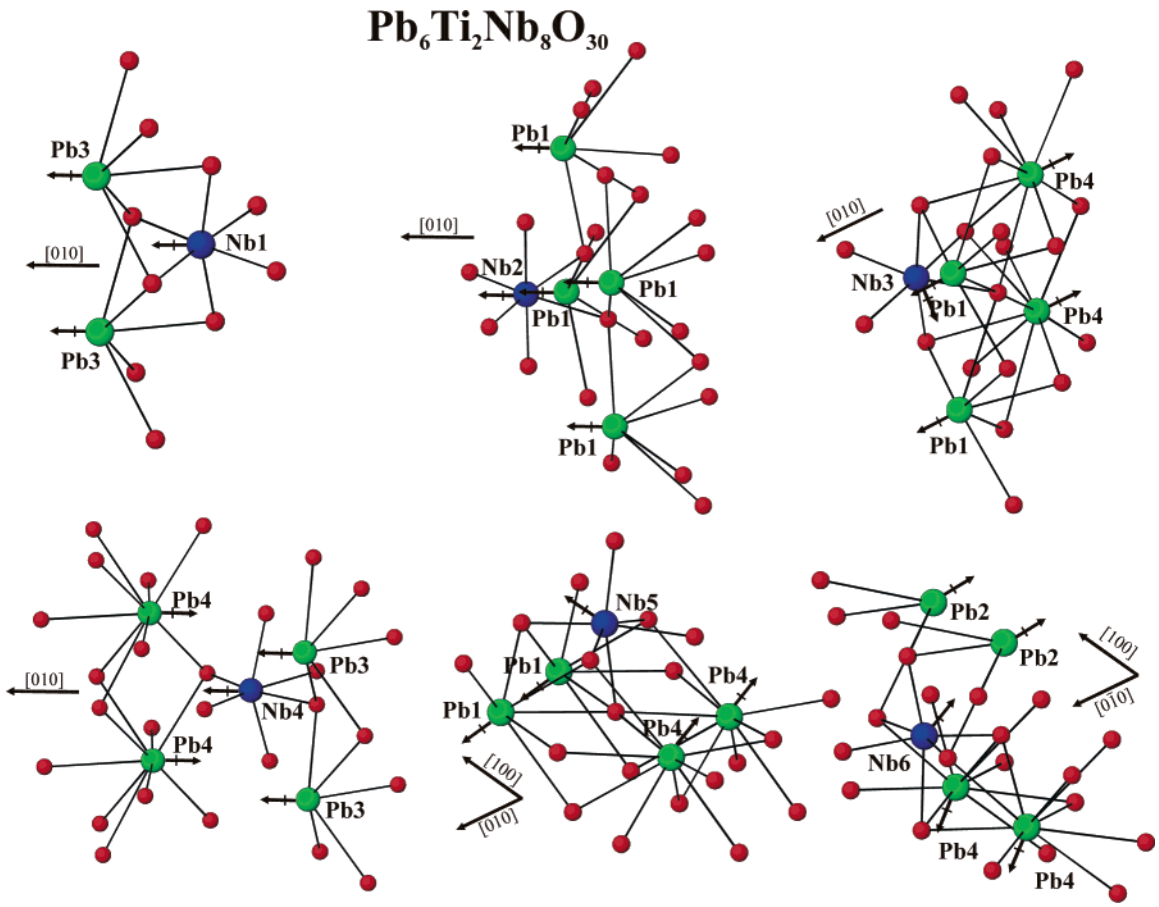

Figure 5. Ball-and-stick representations of the out-of-center distortions of the Ti^{4+}/Nb^{5+} and Pb^{2+} cations in $Pb_6Ti_2Nb_8O_{30}$. The arrows represent the approximate direction of the local moment in each polyhedron.

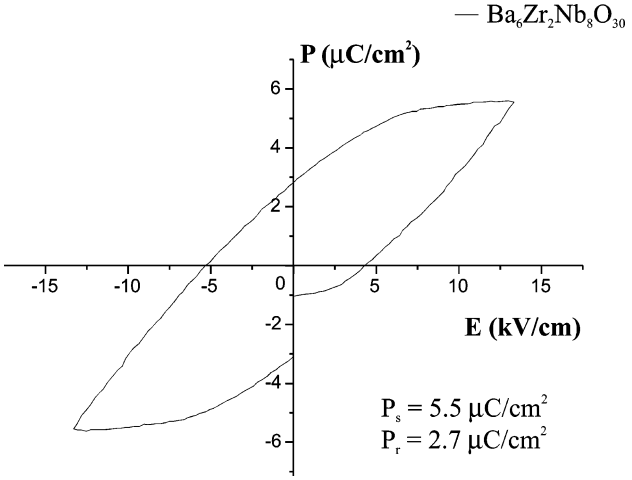

Figure 6. Ferroelectric hysteresis loop (polarization vs electric field) for $Ba_6Zr_2Nb_8O_{30}$.

Dielectric and Ferroelectric Measurements. The changes in the dielectric constant for all nine materials were measured at variable temperatures (−200 to 450 °C) and frequencies (10 and 100 kHz, 1 MHz). The plots of dielectric constant vs temperature for the reported materials have been deposited in the Supporting Information. With $Sr_6Ti_2Nb_8O_{30}$ and $Ba_6Ti_2Nb_8O_{30}$, dielectric maxima were observed consistent with a first-order phase change. The dielectric maxima indicate Curie temperatures of 160 °C ($Sr_6Ti_2Nb_8O_{30}$) and 230 °C ($Ba_6Ti_2Nb_8O_{30}$). The latter value is consistent with previous reports.[5] For all of the other materials, similar dielectric phenomena were not observed up to 450 °C, the maximum temperature of our instrumentation. Ferroelectric measurements, i.e., hysteresis loops (polarization vs electric field) were also performed on all nine materials. All of the reported materials exhibited hysteresis, confirming that the materials are indeed ferroelectric. The spontaneous (P_s) and remnant (P_r) polarization values were determined for each material (see table below). The hysteresis loop for $Ba_6Zr_2Nb_8O_{30}$ is given in Figure 6, whereas for the remaining eight materials the hysteresis loops have been deposited as Supporting Information.

compound	P_s (μC/cm^2)	P_r (μC/cm^2)
$Sr_6Ti_2Nb_8O_{30}$	9.8	6.8
$Sr_6Ti_2Ta_8O_{30}$	1.6	0.4
$Ba_6Ti_2Nb_8O_{30}$	7.1	5.9
$Ba_6Ti_2Ta_8O_{30}$	0.8	0.7
$Ba_6Zr_2Nb_8O_{30}$	5.5	2.7
$Ba_6Zr_2Ta_8O_{30}$	1.6	0.7
$Ba_6Hf_2Nb_8O_{30}$	12.1	5.7
$Ba_6Hf_2Ta_8O_{30}$	1.1	0.9
$Pb_6Ti_2Nb_8O_{30}$	1.4	0.9

Discussion

The M, M′, and Pb^{2+} cations are in asymmetric coordination environments attributable to SOJT effects. The SOJT effects result in an intraoctahedral distortion, for the M and M′ cations, and a lone pair, for the Pb^{2+} cation. Equally important as the local distorted environment and the magnitude of the distortion is the net direction of the distortion. In other words, if all of the distortions are summed, what is the resultant direction? As we will demonstrate, all aspects of the distortions greatly influence the SHG efficiency and ferroelectric polarization.

The SHG efficiencies of the reported materials range from 10 to 600 × SiO_2. If we examine the materials and the SHG responses more closely, some very interesting trends occur. We determined that $Pb_2Ti_6Nb_8O_{30}$ (SHG) > $Ba_6Ti_2Nb_8O_{30}$ (SHG) > $Sr_6Ti_2Nb_8O_{30}$ (SHG). This trend can be explained by examining the local and net distortions of the cations in each material. With the weakest SHG material, $Sr_6Ti_2Nb_8O_{30}$, the out-of-center distortion of the Ti^{4+}/Nb^{5+} cations are quite small, less than 0.08 Å. In addition, the three unique cations displace along the approximate [001], [−1−11], and [−11−1] direction respectively, resulting in a net polarization along the [−101] direction (see Figure 3). For $Ba_6Ti_2Nb_8O_{30}$, the analogous distortions are much larger, ∼0.2 Å, and produce a net polarization along the [001] direction (see Figure 4). Thus, not only do the out-of-center distortions in $Ba_6Ti_2Nb_8O_{30}$ constructively add to a greater extent, compared with $Sr_6Ti_2Nb_8O_{30}$, but the magnitude of the distortions is larger. Thus, it is the constructive addition of the polarizations as well as their magnitude that results in $Ba_6Ti_2Nb_8O_{30}$ (SHG) > $Sr_6Ti_2Nb_8O_{30}$ (SHG). For $Pb_2Ti_6Nb_8O_{30}$, we have an additional polarizable cation, Pb^{2+}. When the Pb^{2+} polarizations are added to the polarizations attributable to the Ti^{4+}/Nb^{5+} cations, we observe constructive addition of both polarizations resulting in a net moment along the [010] direction (see Figure 5). This constructive addition results in $Pb_2Ti_6Nb_8O_{30}$ exhibiting a larger SHG efficiency compared with $Ba_6Ti_2Nb_8O_{30}$.

We also determined that the Nb^{5+} phases have SHG efficiencies greater than the isostructural Ta^{5+} materials, i.e., $Ba_6Ti_2Nb_8O_{30}$ > $Ba_6Ti_2Ta_8O_{30}$, $Ba_6Zr_2Nb_8O_{30}$ > $Ba_6Zr_2Ta_8O_{30}$, $Ba_6Hf_2Nb_8O_{30}$ > $Ba_6Hf_2Ta_8O_{30}$, and $Sr_6Ti_2Nb_8O_{30}$ > $Sr_6Ti_2Ta_8O_{30}$. In addition, if we examine the SHG efficiencies with respect to the M cations, we notice that the materials containing Ti^{4+} (SHG) > Zr^{4+} (SHG) ∼ Hf^{4+} (SHG), i.e., $Ba_6Ti_2Nb_8O_{30}$ > $Ba_6Zr_2Nb_8O_{30}$ ∼ $Ba_6Hf_2Nb_8O_{30}$. For these isostructural compounds the local and net direction of the distortion are the same. Thus, these differences in SHG efficiencies are attributable to the metal−oxygen hyperpolarizabilities of the cations in question. In other words, β(Nb−O) > β(Ta−O) and β(Ti−O) > β(Zr−O) ∼ β(Hf−O). This trend is consistent with earlier reports.[28]

As previously stated, all nine materials are ferroelectric as demonstrated by hysteresis loops. The most important measurement that can be performed on a ferroelectric material is the determination of a hysteresis loop (polarization vs electric field).[20] The full details of a ferroelectric hysteresis loop have been extensively discussed,[20,29] so only a brief description will be given here. Several points of the loop are of interest, the spontaneous (P_s) and remnant (P_r) polarization, the coercive field (E_c), and the shape of the loop. In a ferroelectric, when all of the dipole moments are aligned, the material is considered saturated, since an increase in electric field will not increase the polarization. The

(28) Goodey, J.; Broussard, J.; Halasyamani, P. S. *Chem. Mater.* **2002**, *14*, 3174.
(29) Lines, M. E.; Glass, A. M. *Principles and Applications of Ferroelectrics and Related Materials*; Oxford University Press: Oxford, 1991.

linear extrapolation of the curve back to the polarization axis represents the spontaneous polarization ($+P_s$). As the electric field is reduced from its maximum positive value to zero, some of the dipole moments will remain aligned, and a remnant polarization ($+P_r$) is exhibited. As the external electric field spans the range from its maximum positive to negative value, $-P_s$ and $-P_r$ will be observed. Structurally, all of the dipole moments have switched from the positive to the negative. The "switchability" of a ferroelectric is the basis for its many technological uses.[30] Other information that can be obtained from a ferroelectric hysteresis loop includes the coercive field (E_c) and the shape of the loop. The coercive field is the magnitude of the external electric field necessary to remove all the remnant polarization. The E_c as well as the shape of the loop, i.e., "squareness" or sharpness, are sample dependent and are influenced by grain size and homogeneity.[20]

For the materials reported, the ranges of P_s and P_r are not as varied compared with the SHG efficiencies. It should be noted, however, that we were unable to reach polarization saturation for any of the materials during our measurements owing to the maximum voltage (4000 V) of our instrumentation, as well as the "leakiness" of the compounds. Unlike the SHG efficiencies, adding an additional polarizable cation, Pb^{2+}, does not increase the measured polarization. In fact, we observe a decrease in P_s for $Pb_6Ti_2Nb_8O_{30}$ compared with $Sr_6Ti_2Nb_8O_{30}$ and $Ba_6Ti_2Nb_8O_{30}$. Previously reported hysteresis measurements on ferroelectric Pb^{2+} materials, revealed P_s values in excess of 25 μC/cm^2.[31] In fact, similar to the SHG efficiencies, we expected the P_s of $Pb_6Ti_2Nb_8O_{30}$ to be larger than that of the analogous Sr^{2+} and Ba^{2+} phases. This expectation is attributable to the polarizations of both the Pb^{2+} and Ti^{4+}/Nb^{5+} cations that result in a net moment along the polar [010] direction. The observed lower P_s in $Pb_6Ti_2Nb_8O_{30}$ compared with $Sr_6Ti_2Nb_8O_{30}$ and $Ba_6Ti_2Nb_8O_{30}$ is likely attributable to the fact that we were unable to reach polarization saturation in any of our measurements. Similar to the SHG efficiencies, however, the compounds that contain Nb^{5+} have larger P_s and P_r compared with the isostructural Ta^{5+} compounds, e.g., $Ba_6Ti_2Nb_8O_{30}$ (P_s) > $Ba_6Ti_2Ta_8O_{30}$ (P_s). When Nb^{5+} is a "constant", we notice that materials containing Ti^{4+} have larger polarizations than materials containing Zr^{4+}, e.g., $Ba_6Ti_2Nb_8O_{30}$ (P_s) > $Ba_6Zr_2Nb_8O_{30}$ (P_s). Interestingly, with Hf^{4+} we measured a moderate increase in polarization. When Ta^{5+} is a constant, a change in the M^{4+} cation does not produce a substantial change in polarization, i.e., $Ba_6Ti_2Ta_8O_{30}$ (P_s) ~ $Ba_6Zr_2Ta_8O_{30}$ (P_s) ~ $Ba_6Hf_2Ta_8O_{30}$ (P_s).

Conclusion/Future Work

We have reported on the synthesis and structure−property relationships of nine tungsten bronze-type oxides. All of the materials are not only SHG active but also exhibit ferroelectricity as well. When the A cation is changed to the polarizable Pb^{2+}, the SHG efficiency increases. The compounds that contain Ti^{4+}/Nb^{5+} have larger SHG efficiencies and polarizations compared to Ti^{4+}/Ta^{5+} materials. In addition, the SHG efficiency of the materials with Ti^{4+}/Nb^{5+} is greater than the compounds containing Zr^{4+}/Nb^{5+} and Hf^{4+}/Nb^{5+}. The trends in SHG and ferroelectric behavior seem to scale with the electronegativity of the cation.[32] There are a number of additional experiments that can be done, including high-temperature neutron diffraction. These measurements will allow us to better determine the atomic occupancies of the B1 and B2 sites, as well as describe the nonpolar structures. Additional NCS property measurements are also planned, including pyroelectric and piezoelectric experiments. We plan to develop structure−property relationships with these phenomena as well.

Acknowledgment. We thank the Robert A. Welch Foundation for support. This work was also supported by the NSF-Career Program through DMR-0092054 and an acknowledgment is made to the donors of the Petroleum Research Fund, administered by the American Chemical Society, for partial support of this research. P.S.H. is a Beckman Young Investigator. We also acknowledge Dr. Yaping Li for assistance with the neutron data. Work performed at Argonne is supported by US DOE-BES under Contract No. W-31-109-ENG-38.

Supporting Information Available: Experimental, calculated, and difference diffraction plots, atomic coordinates, metal−oxygen bond lengths, phase-matching data, dielectric data, and ferroelectric hysteresis plots. This material is available free of charge via the Internet at http://pubs.acs.org.

CM049234Y

(30) Auciello, O.; Scott, J. F.; Ramesh, R. *Phys. Today*, **1998**, *40*, 22−27.

(31) Camlibel, I. *J. Appl. Phys*. **1969**, *40*, 1690−1693.

(32) Eng, H. W.; Barnes, P. W.; Auer, B. M.; Woodward, P. M. *J. Solid State Chem*. **2003**, *175*, 94−109.